Journal of Catalysis **200,** 106–116 (2001)
doi:10.1006/jcat.2001.3204, available online at http://www.idealibrary.com on IDEAL®

Characterization and Catalytic Behavior of Co/SiO_2 Catalysts: Influence of Dispersion in the Fischer–Tropsch Reaction

Arnaud Barbier,*,[1] Alain Tuel,*,[2] Iztok Arcon,†,‡ Aloz Kodre,‡,§ and Guy Antonin Martin*

*Institut de Recherches sur la Catalyse, CNRS, Villeurbanne, France; †Nova Gorica Polytechnic, Vipavska 13, 5000 Nova Gorica, Slovenia; ‡Institute Jozef Stefan, Jamova 39, 1000 Ljubljana, Slovenia; and §Faculty of Mathematics and Physics, University of Ljubljana, Jadranska 19, 1000 Ljubljana, Slovenia

Received October 2, 2000; revised January 22, 2001; accepted January 22, 2001; published online April 18, 2001

The study of hydrogen evolution from temperature-programmed desorption (TPD) experiments appears to be so complex that it casts some doubt on the reliability of chemisorption techniques for the estimation of cobalt dispersion in a series of Co/SiO_2 catalysts. Co particle sizes were examined by magnetic measurements (MMs), transmission electron microscopy (TEM), and extended X-ray absorption fine structure (EXAFS). EXAFS shows that Co in the catalysts crystallizes in fcc crystal lattice and that relatively small clusters are formed. The deduced average size is almost an order of magnitude smaller than that obtained by MMs and TEM, suggesting a complex morphology of Co particles. Study of size sensitivity in the Fischer–Tropsch reaction shows that intrinsic activity and chain growth probability first increase and then stabilize on increasing the particle size, thus providing a quantitative determination of the critical diameter separating these two zones, i.e., ca. 6 nm. Study of the surface species after reaction by TPH experiments indicates that (i) deactivation may be due to a loss of catalytically active cobalt; (ii) in the course of the reaction, neither formates nor acetates are detected in the catalyst; and (iii) four carbon-containing species are observed (α, β, γ, and δ). Species β has been speculated to be the active phase of the reaction on the basis of its parallel variation with intrinsic activity. This intermediate, which is strongly interacting with the cobalt phase, does not contain oxygen atoms. The δ species might be associated with graphitic residue formation, whereas no specific role has been attributed to the γ species.

INTRODUCTION

The Fischer–Tropsch synthesis whereby liquid aliphatic hydrocarbons and oxygenates are produced by the hydrogenation of carbon monoxide has been known for about 75 years. Cobalt-containing catalysts are known to be effective in this reaction. The sensitivity of this reaction to Co particle size, however, is not well understood. For Co/SiO_2 catalysts, the absence of any significant particle size effect in the range 6–20% dispersion observed by Ho *et al.* (1) at atmospheric pressure contrasts with a former study by Reuel and Bartholomew (2), who reported an increase in the turnover frequency by a factor of 3 on decreasing dispersion from 20 to 10% under similar conditions and using the same type of catalyst. The invariance of the intrinsic activity has been confirmed by Iglesia *et al.* (3) over the range 3.2–9.5% at 2000 kPa. Literature data show that chain growth probability increases with cobalt particle size (4, 5), whereas this parameter is invariant for large particle sizes (3). Moreover, the influence of cobalt particle size on the stability of the catalyst is not documented.

The uncertainty in the size sensitivity of a reaction may be related to the limits or to the ambiguity of the method used for determining particle size. Reuel and Bartholomew (6) have recommended hydrogen adsorption as the most convenient reliable technique to measure cobalt particle size. This conclusion was based on a comparison between chemisorption data and transmission electron microscopy results or BET surface area measurements performed on a series of supported and unsupported catalysts, respectively. This technique is now widely used to characterize cobalt dispersion. We have previously reported (7) that the surface average diameters calculated by magnetic techniques are in good agreement with those obtained by transmission electron microscopy for a series of Co/SiO_2 catalysts prepared by the ammonia method and having average sizes in the range ca. 4–10 nm. Extended X-ray absorption fine structure (EXAFS) spectroscopy, which provides structural information on the local order around a selected type of atom (8), can be used to characterize the arrangement of metal atoms in dispersed metal catalysts. Crystal structure of metallic clusters and their average size can be deduced from EXAFS data (9–11). However, EXAFS is not a direct method for particle size determination, the average size being obtained from the average number of neighbors, with

[1] Present address: IUT of Rouen, LASTSM, Mont Saint-Aignan, France.

[2] To whom correspondence should be addressed at Institut de Recherches sur la Catalyse, CNRS, 2, avenue A. Einstein, 69626 Villeurbanne Cedex, France. Fax: (+33) (0)4 72 44 53 99. E-mail: tuel@catalyse.univ-lyon1.fr.

0021-9517/01 $35.00

an assumption on the particle shape. Corrections for partial disorder at the surface of clusters have been used (12, 13) to reconcile the size estimates with results of other methods.

The aim of this paper is to examine a series of well-characterized Co/SiO_2 catalysts prepared according to the ammonia method as described in Ref. (7) to gain a better understanding of the size sensitivity in the Fischer–Tropsch reaction with respect to activity, selectivity, and stability. For this purpose, temperature-programmed hydrogenation (TPH) of species present in the catalysts and magnetic measurements were carried out to better define the catalytic systems under reaction conditions. In addition, EXAFS measurements were performed to gain further insight into the intimate morphology of cobalt particles. Data obtained by the different techniques are discussed and a model is proposed to explain the apparent discrepancy observed between data obtained by EXAFS and other techniques.

CATALYST PREPARATION AND CHARACTERIZATION

Samples 1 to 4 were prepared using the ammonia method as described elsewhere (7). Typically, a solution of cobalt(II) nitrate protected from air by an argon blanket was first prepared. After stirring, a 22 wt% solution of ammonia was added dropwise followed by silica (Aerosil 200 from Degussa, 200 m^2/g). After pH equilibrium, the system was centifuged, washed several times, and finally dried in a vacuum oven at 353 K overnight. The precursor was reduced in flowing hydrogen (60 L h^{-1} g^{-1}) by slowly increasing the temperature at a heating rate of 1.3 K/min for 8 h. Samples were held at the final temperature (923 K) for 2 h. Magnetic experiments aimed at characterizing the reduced Co/SiO_2 catalysts thus obtained were performed *in situ* in an electromagnet with fields up to 21 kOe (2.1 T) at 300 K using the Weiss extraction method. These experiments give interesting information on cobalt characteristics, as described elsewhere (7). The amount of reduced cobalt in the metallic state is obtained by comparing the saturation magnetization of the sample with that of bulk Co. The corresponding ratio, F, yields the extent of reduction. It has been shown that under our reduction conditions, the precursors obtained by the ammonia method are completely reduced (7).

Furthermore, when superparamagnetism occurs (no remanence after saturation) average diameters of cobalt particles can be calculated from the variations in magnetization with field strength at low and high fields (D_1 and D_2, respectively). The surface average diameter, D_s, is then defined as $D_s = (D_1 + D_2)/2$. It has been shown that surface average diameters thus obtained are in good agreement with those calculated from transmission electron microscopy (7). The D_s values for samples 1–3 are reported in Table 1. The surface average diameter for sample 4, which is not superparamagnetic, has been obtained by electron microscopy (Table 1).

TABLE 1

Cobalt Loading and Surface Average Diameters as Obtained from Magnetic Measurements (MMs) and Transmission Electron Microscopy (TEM) for Samples 1–5[a]

			D_s (nm)	
Sample	Method	Co (wt%)	MM	TEM
1[b]	Ammonia	3.2	3.8	
2	Ammonia	8.4	5.5	
3	Ammonia	8.2	6.2	
4	Ammonia	19.2		9.2
5	Fluoride	1.83	5.0	

[a] Reduction was carried out in flowing hydrogen (6 L h^{-1}) by slowly increasing the temperature at a heating rate of 1.3 K min^{-1} for 8 h. The final standard temperature was 923 K.

[b] For catalytic experiments a new batch has led to the following characteristics: cobalt loading, 3.5 wt%; surface average diameter, 4.4 nm.

Sample 5 was prepared by reacting a fluoride precursor with silica. This original method is an extension of that proposed to obtain well-dispersed Ti/SiO_2 catalysts (14). Cobalt(III) fluoride (0.193 g) was added to a solvent (diglyme, 2-methoxyethyl ether) and the mixture was heated at 333 K for 30 min in a glass flask equipped with a cooling column. After dissolution of the cobalt fluoride, 5 g of silica (Aerosil 800 from Degussa, 800 m^2/g) was added and stirring was maintained at 333 K for 2 h. The solid phase was filtered and dried in a vacuum oven at 393 K overnight. The precursor was reduced under conditions similar to those used for samples 1–4 except that the final reduction temperature was 1023 K. Magnetic measurements have shown that the precursor of sample 5 is less reducible than those of samples 1–4: in the former, the extents of reduction are 0, 80, 82, 85, and 87% at 473, 560, 703, 910, and 1023 K, respectively. When the reduction is carried out at 1023 K, the cobalt particle size D_s is found to be 5 nm, as measured by magnetic measurements (Table 1). In contrast to samples 1–4, sample 5 is not reoxidized when contacted with air at 300 K. Furthermore, this solid does not show any catalytic activity, suggesting that cobalt particles are embedded in silica.

EXAFS spectra at the Co K edge were measured at EXAFS II station in HASYLAB at DESY. The station provides a focused beam from an Au-coated mirror and a Si(111) double-crystal monochromator with 1.5-eV resolution at the Co K edge. Harmonics are effectively eliminated by a plane Au-coated mirror and by a slight detuning of the monochromator crystals, keeping the intensity at 60% of the rocking curve with the beam stabilization feedback control. Due to the low concentration of cobalt in the samples, about 1 mm of powder was compressed into a liquid absorption cell with Kapton windows to obtain a homogeneous layer with a total absorption thickness of 1.5

above the Co *K* edge, with a Co *K*-edge jump of ca. 0.5. The empty absorption cell served as the reference spectrum under identical conditions. The EXAFS spectrum of Co metal foil was also measured for comparison.

CATALYSIS AND TEMPERATURE-PROGRAMMED HYDROGENATION

The Fischer–Tropsch reaction was carried out in a fixed-bed reactor at atmospheric pressure using 1 g of catalyst reduced *in situ* under standard conditions (conversion less than a few percent). Gases were analyzed on-line by gas chromatography (FID and TCD) at the reactor outlet. The feed ratio CO/H_2 was 0.5. The CO gas flow per cobalt weight was 0.1 mL min^{-1} g^{-1}. The reaction temperatures were successively 443, 453, 463, and 473 K; the catalyst was held at each temperature for 2 h. The deactivation was estimated from the loss of activity at 453 K for 24 h. After reaction, the catalyst was cooled down at room temperature in a helium flow, then heated to 1023 K at a heating rate of 20 K/min in a mixture of hydrogen (3%) and argon with a flow rate of 60 mL/min. The gas composition at the outlet of the reactor was continuously analyzed in a VG-quadrupole mass spectrometer. The most abundant reaction products were H_2O, CH_4, and CO. Small amounts of CO_2, C_2H_6, and C_3H_8 were also detected, whereas O_2 and CH_3OH were not detected. A series of temperature-programmed desorptions (TPDs) of hydrogen were also performed on reduced samples before reaction. The experimental conditions were similar to those for TPH, except that the argon flow was free of hydrogen.

RESULTS

Cobalt Dispersion from Hydrogen TPD

The hydrogen temperature desorptions performed on samples 1, 3, and 4 show three sets of peaks at low, medium, and high temperature (l, m, and h, respectively) (Fig. 1). The m peak is observed only for sample 1. The atomic ratio $N_x = H/Co_s$ (where H is the number of hydrogen atoms, Co_s the number of surface cobalt atoms as calculated from D_s, assuming a cubo-octahedral shape, and *x* the hydrogen peak nature) depends on the size of cobalt particles and is found to be smaller than unity (Fig. 2). N_l goes through a maximum for $D_s = 6.2$ nm while N_h decreases linearly when D_s increases. $N_{(l+m+h)}$ decreases by a factor of 5 when D_s increases from 4 to 9 nm. These results show that the evaluation of cobalt particle size by hydrogen chemisorption, frequently used in the literature, leads to unreliable results.

EXAFS

The EXAFS spectra were analyzed by the UWXAFS code (15, 16) in the *K* range 5–12 $Å^{-1}$, using k^3 weight and a Hanning window. The k^3-weighted Co *K*-edge EXAFS spectra of samples 1, 4, and 5 are shown in Fig. 3. Fourier transforms of the EXAFS spectra (Fig. 4) show the typical local structure of metallic Co. Comparison with the spectrum measured on Co metal foil reveals the same pattern of neighbors. However, the size of individual neighbor peaks is lower than in the Co foil, suggesting that the average number of neighbors is decreased and hence that clusters of Co metal are formed. From the observed reduction of the average number of neighbors, the size of the clusters can be deduced (9–11). For sample 1, an estimate of the size can also be given by the cutoff in the FT spectrum: the absence of a prominent peak observed at 7.5 Å in the FT spectrum of bulk Co provides an upper limit.

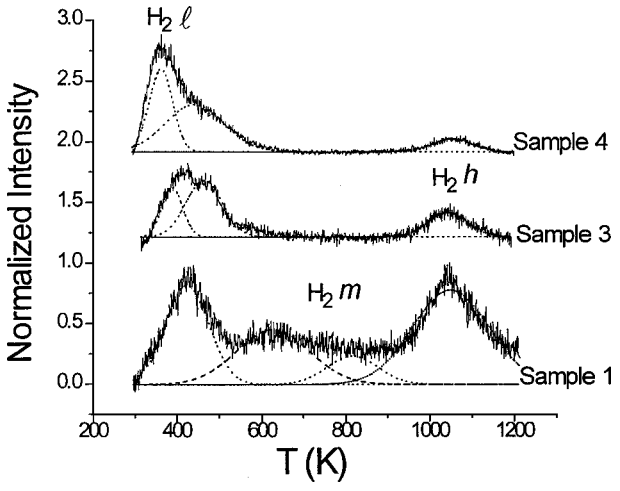

FIG. 1. Profiles of hydrogen temperature-programmed desorption for samples 1, 3, and 4: normalized intensity as a function of the TPD temperature.

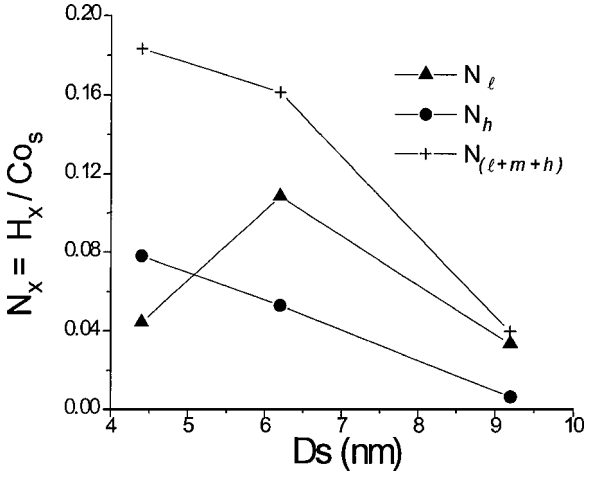

FIG. 2. Atomic ratio $N_x = H_x/Co_s$ (where H is the number of hydrogen atoms, Co_s the number of surface cobalt atoms as calculated from magnetic measurements, and *x* refers to the hydrogen peak nature, *l* (▲), *h* (●), or $l + m + h$ (+)) as a function of the surface average diameter (D_s).

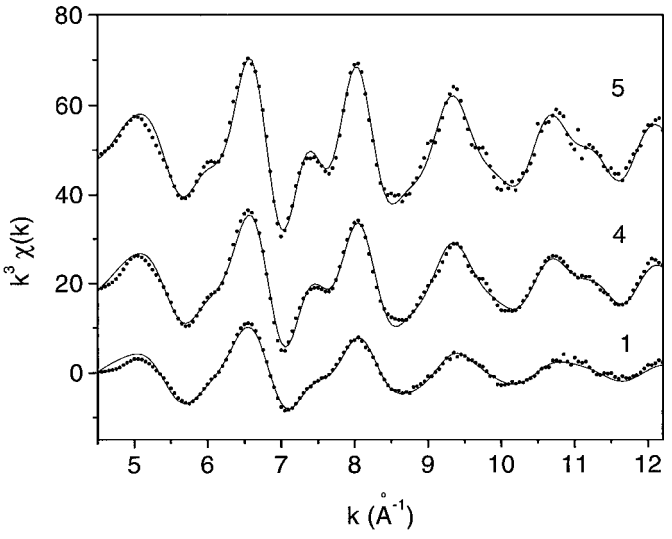

FIG. 3. k^3-weighted Co *K*-edge EXAFS spectra of samples 1, 4, and 5. Dots, experiments; solid line, fit.

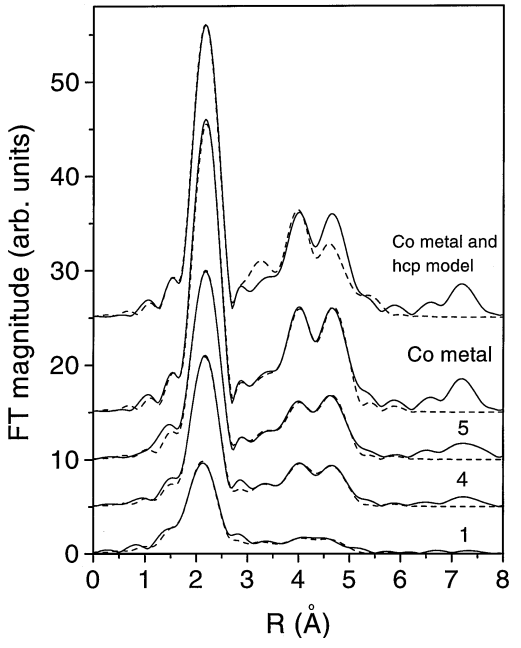

FIG. 4. k^3-weighted Fourier transform magnitude of Co *K*-edge EXAFS spectra of Co metal foil and samples 1, 4, and 5. Solid line, experimental; dashed line, fcc model. With the spectrum of Co foil, the hcp model is also shown (upper spectrum).

To describe the clusters, FEFF models (15) of both known Co metal lattices, fcc and hcp, are constructed. The two lattices differ only in the stacking order of dense (fcc 111) planes, so that the immediate neighborhood of an atom is the same in both, and the differences arise only in parameters of the second and further neighbors. The fcc model with the lattice constant $a = 3.61$ Å comprises the four shortest single scattering paths of the lattice and all multiple scattering paths up to 5.8 Å. The same range of scattering paths is used in the hcp model ($a = 2.51$ Å, $c = 4.07$ Å). The Co foil spectrum is used to calibrate the models. For fcc, an excellent fit is obtained in the region between 1.5 and 5.0 Å with only four variable parameters: the lattice expansion ($\Delta r/r$), the Debye temperature (DT) in modeling the Debye–Waller factors (σ^2) of all paths (17), a separate σ_1^2 for the first-neighbor shell, and the amplitude reduction factor (S_0^2). The shell coordination numbers and radius ratios are fixed at their fcc values. For the hcp model, agreement with experimental spectra in the first-neighbor peak is perfect but further peaks show a significant discrepancy (Fig. 4). We take this fact as proof of the fcc lattice in the calibrating Co foil and, consequently, in the samples.

In modeling the clusters, the fixed value of S_0^2 (0.86(3)) is retained, while DT, σ_1^2 and $\Delta r/r$ are varied, and the fcc shell coordination numbers in the model are multiplied by variable average neighbor fractions (n_i). The accuracy of the results for the variable parameters of the model (Table 2) is supported by the good agreement with data (Fig. 4). For sample 1, an additional shell containing on average 0.8(3) oxygen atom at $r = 1.97(3)$ Å with $\sigma^2 = 0.004(1)$ Å^2 has to be introduced for a fit of equivalent quality.

TABLE 2

Average Neighbor Fractions (n_i) of Co Neighbors in the First Four Coordination Shells in the Co/SiO_2 Samples [a]

Sample	n_1	n_2	n_3	n_4	$\Delta r/r$	σ_1^2 (Å^2) shell 1	T_D (K) shells 2–4
1	0.52(4)	0.37(8)	0.21(5)	0.15(5)	0.037(4)	0.010(1)	300(90)
4	0.66(5)	0.53(9)	0.42(6)	0.38(8)	0.048(4)	0.0085(6)	350(20)
5	0.72(4)	0.63(6)	0.65(4)	0.64(4)	0.053(4)	0.0074(5)	340(20)
	N_1	N_2	N_3	N_4			
Co metal	12	6	24	12	0.047(4)	0.0068(2)	364(10)

[a] Best-fit values for the lattice expansion ($\Delta r/r$), the Debye–Waller factor of the first coordination shell σ_1^2, and the Debye temperature (T_D) governing the width of further shells are added. The model parameters determined on the reference Co metal foil are added for comparison. Shell coordination numbers N_i were fixed at their fcc values. Uncertainties on the last digit are given in parentheses.

TABLE 3

Model: Average Number Fraction (n_i) of Consecutive Neighbors in fcc Magic-Number Co Clusters

$N_{at/cl}$	Cluster diameter (nm)	n_1	n_2	n_3
13	0.511	0.4615	0.3077	0.1538
19	**0.722**	**0.5263**	**0.3158**	**0.2105**
43	0.884	0.6047	0.5116	0.3721
55	**1.021**	**0.6545**	**0.5455**	**0.4000**
135	**1.351**	**0.7407**	**0.6667**	**0.5481**
201	1.614	0.7861	0.6567	0.6070
344	1.976	0.818	0.737	0.678
380[a]	2.0	0.808	0.729	0.668
1300[a]	3.0	0.870	0.819	0.778
3000[a]	4.0	0.904	0.864	0.834

[a] Analytical estimation of $N_{at/cl}$ and n for a given cluster diameter (from (10)).

The average neighbor fractions (n_i) of the first four shells extracted from EXAFS spectra of the samples are converted into cluster sizes with the following assumption. Model clusters are constructed as fcc magic-number clusters by filling consecutive crystallographic shells, i.e., shells of sites with all permutations of the same crystallographic indices with respect to the central atom. The model neighbor fractions are obtained by summing the number of *i*th neighbors over all atoms of the cluster and dividing by the corresponding number in the bulk (Table 3). The experimental neighbor fractions are compared with the table of values from model clusters of increasing size (Table 3). The best agreement is obtained for clusters containing 19, 55, and 135 atoms (diameters of 0.72, 1.02, and 1.35 nm) for samples 1, 4, and 5, respectively. The agreement in all four shells for the two smaller clusters is remarkable. It is possible that the larger deviation for sample 5 indicates a deformation from the globular shape.

From the sizes obtained it becomes clear why the oxygen neighbors are found only for sample 1. They probably come from the contact layer with the substrate and become visible only for the smallest clusters where most of the Co atoms in the cluster are located on its surface.

Further support for the cluster sizes obtained based on the spherical cluster model is provided by the analysis of Debye–Waller factors and Co–Co distances. An increase in the Debye–Waller factor for the first shell and a corresponding decrease in the DT for more distant shells compared with bulk Co are observed for all samples. The increase in the Debye–Waller factor is higher for smaller clusters and can be ascribed to the increased static part of the disorder in the clusters (11, 17). A smaller reduction of interatomic distances is observed only in the case of small clusters (sample 1), in agreement with similar observations on small Cu clusters (17, 18). Larger clusters found in samples 4 and 5 do not show significant contraction of the interatomic distances compared with bulk Co.

Catalysis

Figure 5 shows the variation in intrinsic activity (turnover frequency (TOF), number of CO molecules converted per surface cobalt atom, as deduced from D_s assuming a cubo-octahedral shape, per second, measured at 453 K) and of the specific activity (number of CO molecules converted per total cobalt atom per second at 453 K) with the surface average diameter of cobalt particles as obtained by magnetic measurements after reaction. The average diameter does not exactly coincide with that reported in Table 1, measured before reaction, probably because some sintering has occurred during reaction. As can be seen, the TOF increases continuously with D_s, first rapidly in the region 4–6 nm, then more slowly from 6 to 9 nm. Chain growth probability, α, is calculated from the slope of the curve $\ln(S_n/n)$ versus n, where n is the carbon number of the hydrocarbon and S_n the corresponding selectivity. As shown in Fig. 6, α increases when the temperature decreases. Furthermore, chain growth probability is an increasing function of cobalt particle diameter: this parameter first increases rapidly and then more slowly for diameters larger than 6 nm.

The influence of cobalt particle size on the rate of deactivation is illustrated in Fig. 7. As D_s increases, this rate first increases, goes through a maximum for $D = 5.5$ nm, and then decreases. Over the range studied, catalysts with a particle size of ca. 10 nm seem to be the most stable.

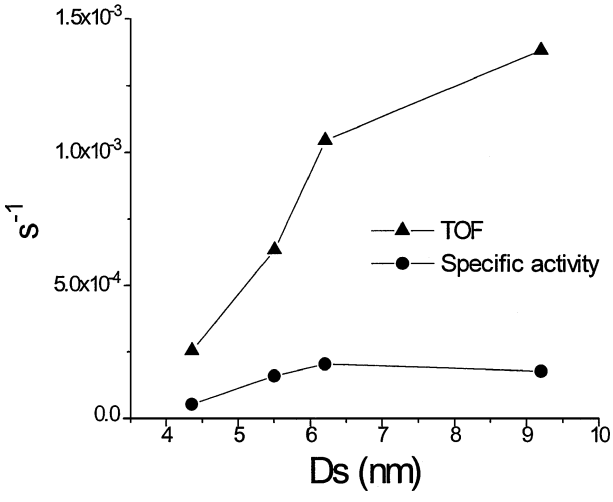

FIG. 5. Variation of the intrinsic activity ((▲), turnover frequency, TOF, number of CO molecules converted per surface cobalt atoms per second measured at 453 K) and the specific activity ((●), number of CO molecules converted per total cobalt atom per second at 453 K) with the surface average diameter (D_s).

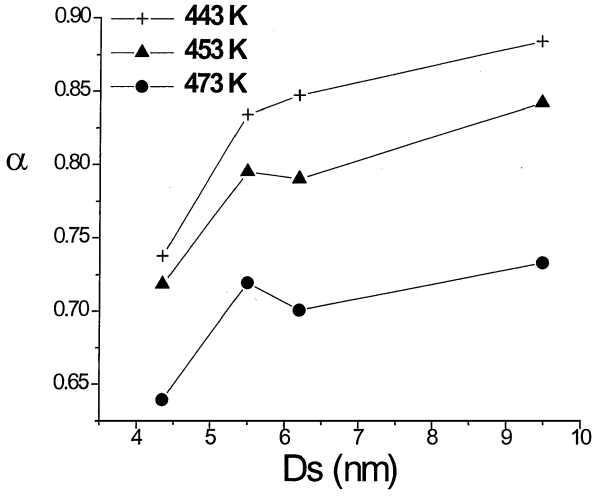

FIG. 6. Variation of chain growth probability (α) at different temperatures (443 K (+), 453 K (▲) and 473 K (●)) with the surface average diameter (D_s).

TPH Analysis of Species Present in Sample 4 after 24 h of Reaction

Figure 8 shows the product evolution of the TPH temperature for sample 4 after 24 h of reaction and Table 4 reports the order of magnitude of the mass spectrometer intensity and the maximum temperature of the signal, T_m. As can be seen, the hydrogen consumption peak (435 K) and the first water evolution peak (440 K) are observed to coincide. Furthermore, the corresponding peak intensities are comparable. This observation strongly suggests that these peaks result from the hydrogenation of oxygen atoms issued from the carbon monoxide dissociation. This reduction takes place at a temperature lower than that corresponding to hydrocarbon evolution (435–440 K vs 451–461 K), suggesting that oxygen atom removal is not the rate-limiting step in the Fischer–Tropsch reaction.

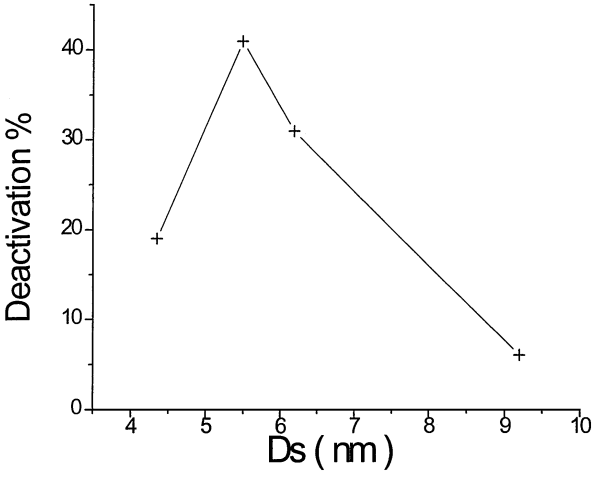

FIG. 7. Deactivation (estimated from the loss of activity at 453 K for 24 h) as a function of surface average diameter (D_s).

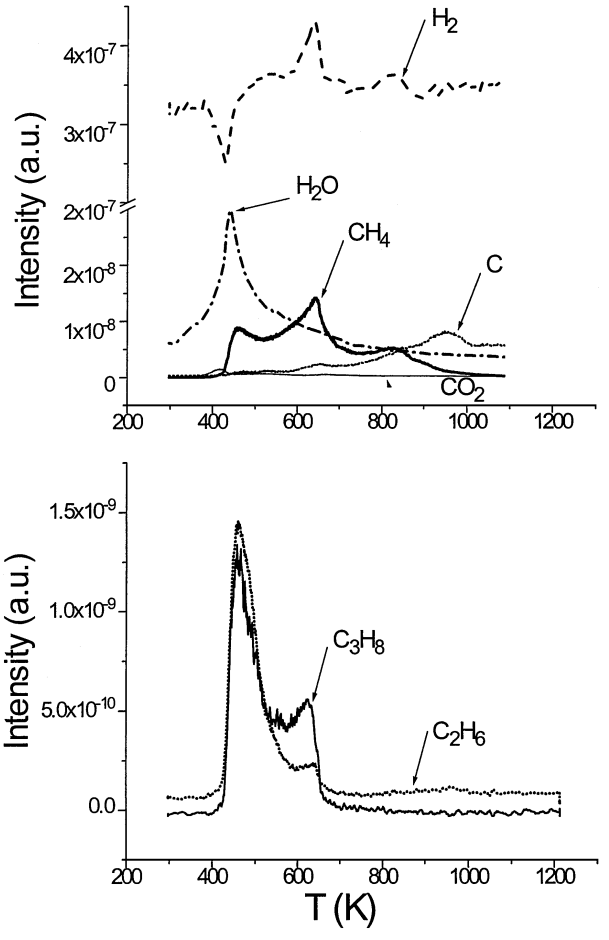

FIG. 8. TPH profiles of sample 4 after 24 h of reaction: intensity in arbitrary units (a.u.) as a function of the TPH temperature.

The origin of hydrogen peak formation at 640 K, which does not correspond to any hydrogen peak desorption in

TABLE 4

Order of Magnitude of the Mass Spectrometer Intensity and Maximum Temperature of the Signal, T_m

	Products	Intensity order of magnitude	T_m (K)
Consumption	H_2	7×10^{-8}	435
Formation	H_2	7×10^{-8}	660
Formation	H_2O	3×10^{-8}	440, 550–650
Formation	CH_4	1.5×10^{-8}	461, 644, 827
Formation	CO	7×10^{-9}	500, 644, 950
Formation	CO_2	1.5×10^{-9}	422, 510, 664
Formation	C_2H_6	1.5×10^{-9}	456, 628
Formation	C_3H_8	1×10^{-9}	451, 619
Formation	O_2	1×10^{-12}	—
Formation	CH_3OH	1×10^{-12}	—

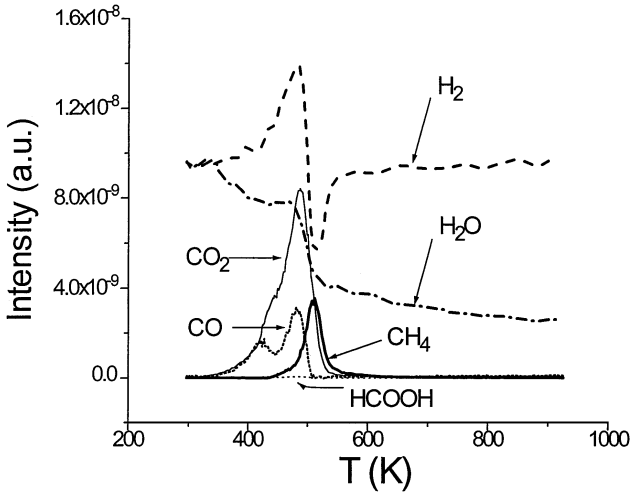

FIG. 9. TPH profiles of sample 4 contacted with formic acid/He at 300 K: intensity in arbitrary units (a.u.) as a function of the TPH temperature.

TPD experiments (Fig. 1) and which may be coincidental with a methane evolution peak (644 K), is not well understood.

The possibility of formate and acetate formation in the course of the reaction has been considered. After reduction, sample 4 was contacted at room temperature with a mixture of helium saturated with formic or acetic acid, then purged with pure helium and submitted to a TPH experiment. With formic acid, the products detected were H_2O, CO_2, CO, CH_4, and H_2 (Fig. 9). A CO_2 peak is observed at 485 K, a double peak of CO at 420 and 480 K, and a methane peak at 515 K, related to a hydrogen consumption peak at 515 K. A hydrogen formation peak at 480 K might correspond to the CO_2 and CO peaks at 485 and 480 K, respectively. A broad peak of water is observed at low temperature, indicative of its accumulation in the catalyst. No C2+ hydrocarbons are detected. The catalyst contacted with acetic acid (Fig. 10) leads to the formation of methane and carbon dioxide, which appear simultaneously at 550 K. This corresponds to the temperature of hydrogen consumption. A broad low-temperature peak of water analogous to that observed with formic acid is also detected along with small amounts of acetic acid. Neither ethane nor propane molecules are detected. As can be seen, the TPH spectra of formate and acetate surface species are very different from that of sample 4, indicating that the former species are more likely not present in the reacting catalyst.

The methane TPH curve can be deconvoluted into four Gaussian peaks a, b, c, and d at ca. 470, 580, 650, and 820 K, respectively (Fig. 11). The corresponding species are denominated α, β, γ, and δ. The ethane and propane profiles, after deconvolution, lead to three peaks at ca. 470, 550, and 630 K; no C2+ are observed at 820 K. These observations suggest that the δ species does not belong to the same family as the α, β, and γ species; the latter, which leads to C2+ hydrocarbons, are good candidates for being reaction intermediates. The specificity of δ species has been confirmed by the following analysis: The TPH experiment was stopped at 513, 606, 682, 873, and 973 K, and the saturation magnetization of cobalt was subsequently measured after cooling the system at 300 K under a flow of pure helium. An increase in the magnetization was observed for the three first temperature intervals (0.7, 4.2, and 1.8%, respectively), whereas no change was observed for the interval 682–973 K. This observation might be explained by assuming that the δ species consists of graphitic carbon, which would not interact with cobalt.

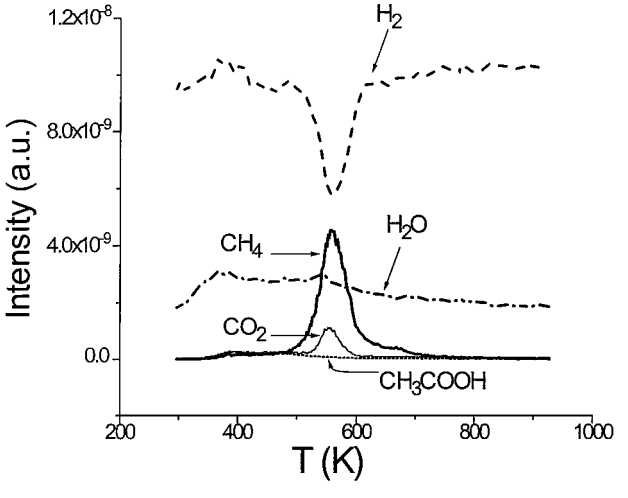

FIG. 10. TPH profiles of sample 4 contacted with acetic acid/He at 300 K: intensity in arbitrary units (a.u.) as a function of the TPH temperature.

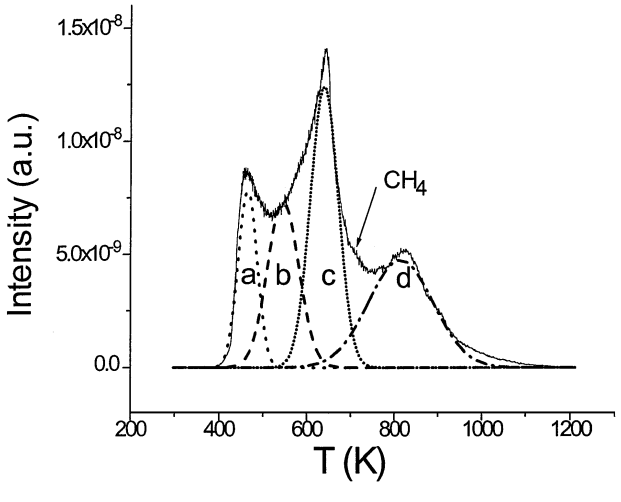

FIG. 11. TPH profile of methane for sample 4 after 24 h of reaction and decomposition of the methane TPH curve into four Gaussian peaks, a, b, c, and d, at ca. 470, 580, 650, and 820 K, respectively: intensity in arbitrary units (a.u.) as a function of the TPH temperature.

Influence of Reaction Time

Figure 12 shows the variations in the normalized intensity of each product with temperature for the three reaction times (the intensity of the maximum peak is taken equal to unity). As can be seen, the TPH curves obtained after 10 min of reaction are very different from those obtained after 3.5 and 24 h; for example, a water production peak is observed at high temperature after 10 min and is no longer detected after 3.5 and 24 h. This peak does not coincide with any carbon oxide production. Furthermore, it corresponds to a small hydrogen consumption. This observation might result from the reduction of a cobalt species not easily reducible such as an anhydrous silicate or a phyllosilicate produced by hydrothermal treatment of the catalyst resulting from the initial overheating in the presence of water formed during the reaction. As reaction time increases, the high-temperature reduction phenomenon disappears and the reduction of the easily reducible species previously described takes place. Variations in the carbon monoxide profile also illustrate the change in catalyst characteristics occurring in the course of the reaction.

Figure 13 shows the variations in the peak intensity of methane with time. The δ species is not observed at short reaction time. Its intensity increases with reaction time. This observation is compatible with our hypothesis that the δ species corresponds to the formation of graphitic deposits accumulating in the catalyst. The evolution of the α, β, and γ species (which lead to C2+ hydrocarbons in contrast with the δ species) is different: the concentration of the α species, the most abundant species at short reaction times, first decreases strongly whereas those of the β and γ species increase. This strongly suggests that the α species is the precursor of the other species. After a time in excess of 3.5 h, the concentrations of α, β, and γ species stabilize.

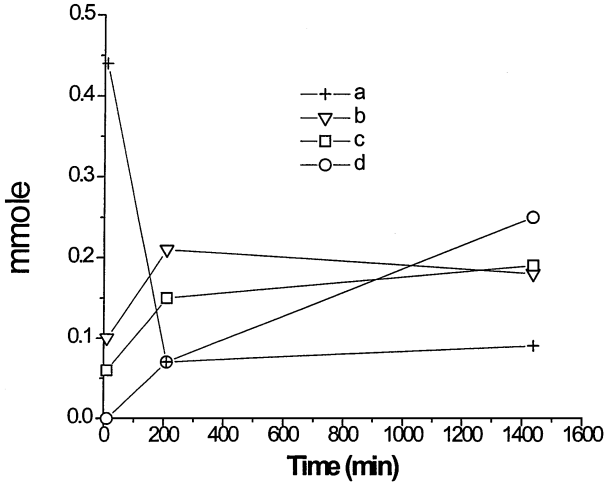

FIG. 13. Variation of the peak intensity of methane (millimoles of methane corresponding to the TPH peaks: a (+), b (▽), c (□), and d (○)) with time.

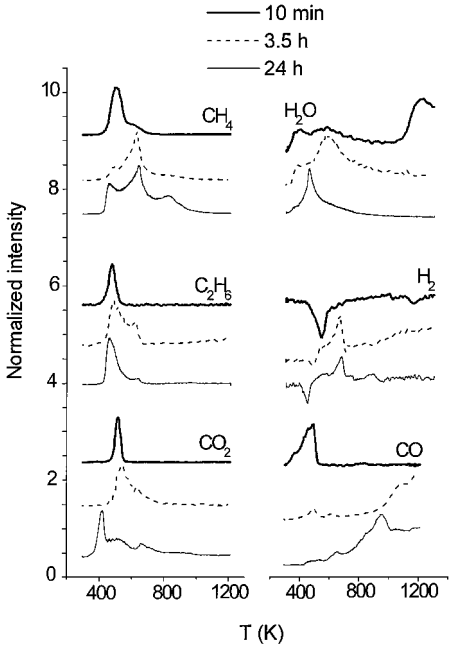

FIG. 12. TPH profiles of H_2O, CO, CH_4, CO_2, C_2H_6, and H_2 for sample 4 after 10 min, 3.5 h, and 24 h of reaction: normalized intensity as a function of the TPH temperature.

Influence of Particle Size on TPH Data

Figure 14 illustrates the TPH profiles of samples 1–4 after 24 h of reaction. The water curve can be decomposed into three Gaussian peaks at 440, 605, and 1120 K. The high-temperature peak is not observed for sample 4, whereas it is present for samples 1–3. This peak, which coincides with hydrogen consumption, is observed for sample 4 after 10 min of reaction and has been assigned to the presence of a cobalt compound not easily reducible such as a silicate or a phyllosilicate. The CO profile goes through three maxima at 480, 640, and 920 K and the CO_2 curve yields four identifiable peaks at 420, 515, 645, and 875 K. The methane curves can be decomposed into four peaks regardless of the cobalt dispersion at ca. 470, 580, 650, and 820 K. The first three peaks are associated with ethane and propane formation, in contrast with the 820 K peak. Figure 15 shows the variation in carbon coverage, R_x, associated with the different carbon species present on the catalyst, with the diameter of the cobalt particles. R_x is equal to the ratio of the number of carbon atoms as calculated from TPH experiments to the number of surface cobalt atoms. The subscript x denotes the peak intensity (a, b, c, and d at 470, 580, 650, and 820 K, respectively). As can be seen, an analogy between the variations in R_b and R_d is observed: the coverages of the β and δ species increase more or less continuously with D.

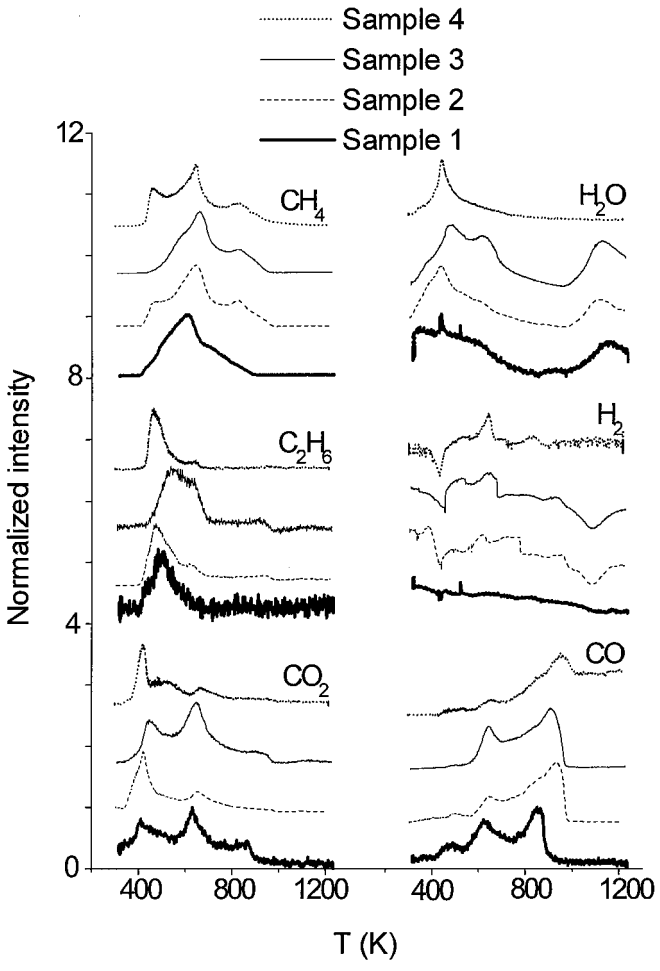

FIG. 14. TPH profiles of H_2O, CO, CH_4, CO_2, C_2H_6, and H_2 for samples 1–4 after 24 h of reaction: normalized intensity as a function of the TPH temperature.

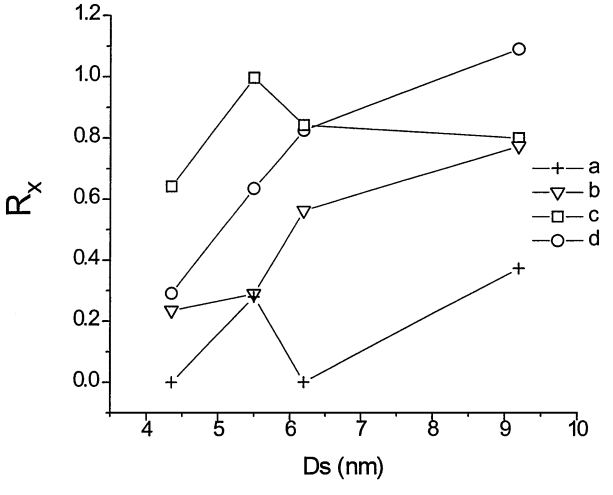

FIG. 15. Variations of the carbon coverage, R_x, associated with the different carbon species present on the catalyst, with surface average diameter (D_s). R_x is equal to the ratio of the number of carbon atoms as calculated from TPH experiments to the number of surface cobalt atoms. The subscript x denotes the peak identity (a (+), b (▽), c (□), and d (●) at 470, 580, 650, and 820 K, respectively).

DISCUSSION

EXAFS

EXAFS shows that Co in samples 1, 4, and 5 crystallizes in the fcc crystal lattice as bulk Co. The average number of Co neighbors in the consecutive coordination shells in the samples is lower than in the Co foil, indicating that clusters with the fcc structure of Co metal are formed. However, the average sizes of the clusters, deduced from the observed reduction in the average number of neighbors, are significantly smaller than those obtained by magnetic measurements or microscopy. Such observations on catalytic samples have been previously reported by different authors (12, 18). An explanation of the discrepancy, besides that cited earlier (12) which employs specific models of disorder at the cluster surface, can be given by an aggregate morphology of Co particles.

It should be emphasized that the directly determined experimental parameter in EXAFS analysis is the average number of neighbors. It is correlated linearly to the fraction of surface atoms in a cluster, as can easily be shown for large clusters: atoms in the core contribute with the full coordination number of neighbors (12 in fcc lattice), whereas those at the surface contribute with a deficient number (9 in fcc). Thus, the average number of (first) neighbors is a direct measure of the specific surface of the dispersed metal, and (should be) is directly related to the catalytic activity. The conclusion is largely independent of the cluster shape and size distribution. The value of the cluster diameter, on the other side, depends critically on the assumptions of uniformity and globular shape. In the other two cases of simple shapes, cylindrical rods and platelets, the extracted size parameter (diameter of rods and thickness of the platelets) would differ for a small numerical factor (2/3 in fcc). However, it would invariably be the small shape parameter; the average number of neighbors is largely insensitive to the large size parameter, i.e., the length of the rods or the width of the platelets. The conclusion can be extended to aggregates of simple shapes (dendrites of globules, rods or platelets) as long as the attachment area is small.

If globular clusters with perfect fcc structure are formed, as assumed in the EXAFS model, then EXAFS is shown to give reliable estimates of the average particle size (9, 10, 18). By contrast, larger aggregates composed of small globular Co crystallites attached to each other by only a small fraction of their surface give the large overall diameters obtained by magnetic measurements or microscopy. For example, samples 1 and 4 prepared in ammonia possess clusters with diameters of ca. 4.4 and 9.2 nm, respectively while the corresponding globule sizes are 0.722 and 1.021 nm.

Tight aggregates are also possible, whereby the small globular clusters assume the role of domains in polycrystalline materials. The EXAFS estimate of the size refers to the region of short-range order within a domain. A

similar model has been previously reported for Ni/SiO_2 catalysts (19) and MoS_2 on oxidic or carbon carriers (12). There is no direct relationship between the size of the domains and those of the large cobalt particles. It is also not clear, however, what mechanism would produce that particular morphology.

Due to the ambiguities of EXAFS models we tried to relate the catalytic activity of the samples to particle diameters and dispersion calculated from magnetic measurements, which give results in good agreement with electron microscopy.

Catalytic Activity

For practicable applications, catalysts yielding the highest conversion associated with the lowest weight of cobalt are desirable. Our results (Fig. 5) show that, from this point of view, the optimal diameter for cobalt particles is close to 6 nm. The corresponding rate of deactivation is, however, large (Fig. 7). Finally, if one tries to reconcile the parameters high specific activity, low rate of deactivation, and high chain growth probability, our data show that Co/SiO_2 catalysts with $D \sim 9$ nm are to be preferred in Fischer–Tropsch synthesis.

Size Sensitivity

The trend toward size insensitivity we observe for the intrinsic activity for diameters larger than 6–9 nm (Fig. 5) agrees well with the data of Ho *et al.* (1) at atmospheric pressure, Iglesia *et al.* (3), and Azib (5) at $P = 2$ MPa, who reported no important variations for diameters in excess of 5, 10, and 9 nm, respectively. Over the low-diameter range, our results are also in qualitative agreement with those of Reuel *et al.* (2), who have reported an increase in activity for cobalt particle diameters larger than 1 nm (dispersion 86%). The use of chemisorption techniques in the latter case casts some doubt on the quantitative aspects of the size determination, however. Furthermore, these authors have used partially reduced catalysts, so their conclusions are not completely unambiguous. In our case, the catalysts are initially fully reduced so that the hypothesis of a possible extent of reduction effect can be discarded to account for the size sensitivity observed. Finally, it can be underlined that our results are very similar to those obtained by Dalmon and Martin (19) on nickel catalysts, where a steep decrease in the intrinsic activity was reported for diameters lower than 6 nm.

The variations in chain growth probability observed in this work (Fig. 6) are also in agreement with literature data: generally, α decreases with dispersion (4–6, 20), whereas a size insensitivity is observed for large particles in the dispersion range 0.45–9.5% (3). Our study provides a quantitative determination of the critical diameter separating these two zones, i.e., 6 nm. The size sensitivity of Co/SiO_2 catalysts is similar to that observed for Ni/SiO_2 catalysts which demonstrate the same behavior (19): the selectivity toward C2+ hydrocarbons increases with nickel particle size, then stabilizes for diameters larger than ca. 6 nm.

Various hypotheses have been proposed to account for the parallel variations in intrinsic activity and chain growth probability with cobalt particle size. More specifically, it has been speculated that the CO coordination could be favored on larger particles (2), thus increasing the CO dissociation rate and the intermediate concentration. Our TPH data (Fig. 14) do not contradict this assumption: the position of the high-temperature peak of CO evolution (probably related to the highly coordinated species) shifts to lower temperatures when cobalt particle size decreases from 9 to 4 nm. It cannot be overlooked, however, that in the case of nickel catalysts that yield the same behavior as cobalt catalysts, the ensemble model accounts for activity and selectivity variations with particle size. These two hypotheses are not mutually exclusive as the highly coordinated CO adsorbed species probably requires an ensemble composed of several adjacent metal atoms as an adsorption site.

Reacting Intermediate

Among the three carbon-containing species leading to a mixture of methane and C2+ hydrocarbons detected by TPH, the β species seems to be related to the reacting intermediate; in fact the variations in its coverage with cobalt particle size parallels that of the intrinsic activity. It is inferred that the β species may be identified with the reacting intermediate of the reaction. The temperature of the peak maximum for β (550 K) does not coincide with that of the oxygenates (H_2O, CO, CO_2), suggesting that this species does not contain oxygen atoms ($[CH_x]_n$). Its hydrogenation leads to the largest magnetic effect (increase in magnetization by 4.2%), confirming that this intermediate is interacting with the metal cobalt phase. Its coverage order of magnitude (0.2–0.3) is comparable to that observed over a similar nickel catalyst by transient kinetics (0.1–0.3) (21). It could be argued that the β species, which leads mostly to methane in TPH experiments, cannot be the reacting intermediate in the Fischer–Tropsch reaction, on the basis that the latter gives heavy hydrocarbons. However, this argument can be rebutted considering that the Fischer–Tropsch reaction and TPH occur under very different experimental conditions. TPH, which is performed at increasing temperatures in the absence of CO, might favor the hydrogenolysis of Cn species into methane, thus explaining the difference in the nature of the products with the Fischer–Tropsch reaction.

Deactivation

The same type of analogy might be found between the deactivation rate and the c coverage related to the γ species (Figs. 7 and 15): both parameters first increase, go through a maximum, and then decrease as cobalt particle

size increases. The parallel, however, is much less quantitative than in the case of the intrinsic activity and the coverage of the β species; in fact, the difference between the extreme values of the c coverage does not exceed 50%, whereas the rate of deactivation varies by a factor of 7 when D increases from 5.5 to 9 nm.

A better clue to identify the main cause of deactivation is provided by careful examination of the TPH curves of water evolving at high temperature, associated with a high-temperature hydrogen consumption peak, revealing the presence of an oxidized cobalt phase not easily reducible (Fig. 14). It is striking to observe that after 24 h of reaction, the most stable catalyst (sample 4, $D_s = 9.2$ nm) does not contain this phase, in contrast with samples 1 to 3, the least stable catalysts. It can be inferred that deactivation is probably due to a loss of catalytically active cobalt, which is oxidized to irreducible cobalt silicate or phyllosilicate in the course of the reaction (22, 24).

CONCLUSION

The formation of Co clusters with the fcc crystal structure in Co/SiO_2 catalysts is definitely established by EXAFS. Estimated average sizes of the clusters deduced from EXAFS data are significantly smaller than those obtained by magnetic measurements or TEM. The observed discrepancy suggests a complex morphology for Co particles. A dendritic or polycrystalline structure of large Co particles, composed of several small individual Co crystallites, is proposed, a situation already met in the case of some Ni/SiO_2 catalysts. Hydrogen evolution from TPH experiments appears to be so complex that it casts some doubt on the reliability of chemisorption techniques for the estimation of cobalt dispersion. The ambiguities of EXAFS and chemisorption methods have led us to use diameters and dispersions calculated from magnetic measurements, which give results in good agreement with electron microscopy, in the presentation of our catalytic results.

The size sensitivity of the Fischer–Tropsch reaction has been confirmed: intrinsic activity (per unit area) and chain growth probability first increase, then stabilize at increasing particle size. Our data provide a quantitative determination of the critical diameter separating these two zones, i.e., ca. 6 nm. A topological hypothesis (high index planes could favor highly coordinated chemisorbed CO) has already been put forward to account for this observation: this possible explanation is not exclusive of that based on the ensemble model proposed for the case of Ni/SiO_2 catalysts which yield the same behavior. The rate of deactivation is also sensitive to cobalt particle size. TPH experiments indicate that deactivation may be due to a loss of catalytically active cobalt, which is transformed into irreducible cobalt compounds under our reacting conditions.

In the course of the reaction, neither formates nor acetates are detected in the catalyst. Four carbon-containing species are observed. The most reactive toward hydrogen, α, is abundant at low reaction time and its concentration decreases with time, whereas the second, β, has been tentatively assigned to the active phase of the reaction on the basis of its parallel variation with intrinsic activity. This intermediate, which is strongly interacting with the cobalt phase, does not contain oxygen atoms. The δ species might be associated with graphitic residue formation, whereas no specific role has been attributed to the γ species.

ACKNOWLEDGMENTS

The EXAFS study is supported by Internationales Buero des BMBF, Germany, and Ministry of Sciences and Technology, Slovenia. Expert advice on the EXAFS 2 beamline operation of M. Tischer from HASYLAB is gratefully acknowledged.

REFERENCES

1. Ho, S. W., Houalla, M., and Hercules, D. M., *J. Phys. Chem.* **94**, 6396 (1990).
2. Reuel, R. C., and Bartholomew, C. H., *J. Catal.* **85**, 78 (1984).
3. Iglesia, E., Soled, S. L., and Fiato, R. A., *J. Catal.* **137**, 212 (1992).
4. Bartholomew, C. H., *Catal. Lett.* **7**, 27 (1990).
5. Azib, H., Thesis, University P. and M. Curie, Paris VI, 1996.
6. Reuel, R. C., and Bartholomew, C. H., *J. Catal.* **85**, 63 (1984).
7. Barbier, A., Hanif, A., Dalmon, J. A., and Martin, G. A., *Appl. Catal. A* **168**, 333 (1998); Barbier, A., Brun-Pereira, E., and Martin, G. A., *Catal. Lett.* **45**, 221 (1999).
8. Rehr, J. J., and Albers, R. C., *Rev. Mod. Phys.* **72**, 621 (2000).
9. Frenkel, A. I., *J. Synchrotron Radiat.* **6**, 293 (1999).
10. Borowski, M., *J. Phys. IV.* **7(C2)**, 259 (1997).
11. kakar, S., Bjorneholm, O., Weigelt, J., De Castro, A. R. B., Troeger, L., Frahm, R., Moeller, T., Knop, A., and Ruehl, E., *Phys. Rev. Lett.* **78**, 1675 (1997).
12. Shido, T., and Prins, R., *J. Phys. Chem. B* **102**, 8426 (1998).
13. Bensaddik, A., Ernst, B., Garin, F., Maire, G., and Kiennemann, A., *J. Phys. IV* **6(C4)**, 545 (1996).
14. Jorda, E., Tuel, A., Teissier, R., and Kervennal, J., *J. Chem. Soc. Chem. Commun.*, 1775 (1995).
15. Rher, J. J., Albers, R. C., and Zabinsky, S. I., *Phys. Rev. Lett.* **69**, 3397 (1992).
16. Stern, E. A., Newville, M., Ravel, B., Yacoby, Y., and Haskel, D., *Physica B*, 117 (1995).
17. D'Acapito, F., Cattaruzza, E., Gonella, F., Mobilio, S., Regnard, J. R., and Spizzo, F. J., *J. Phys. IV* **7(C2)**, 1107 (1997).
18. Montano, P. A., Shenoy, G. K., Alp, E. E., Shulze, W., and Urban, J., *Phys. Rev. Lett.* **56**, 2076 (1986).
19. Dalmon, J. A., and Martin, G. A., *J. Catal.* **84**, 45 (1983).
20. Van de Loosdrecht, J., Van der Haar, M., Van der Kraan, A. M., Van Dillen, A. J., and Geus, J. W., *Appl. Catal. A* **150**, 365 (1997).
21. Agnelli, M., Swaan, H. M., Marquez Alvarez, C., Martin, G. A., and Mirodatos, C., *J. Catal.* **175**, 117 (1998).
22. Coulter, K. E., and Sault, A. G., *J. Catal.* **154**, 56 (1995).
23. Kogelbauer, A., Weber, J. C., and Goodwin J. G., Jr., *Catal. Lett.* **34**, 259 (1995).
24. Van Berge, P. J., Van de Loosdrecht, J., Barradasa, S., and Van der Kraam, A. M., *Catal. Today* **58**, 321 (2000).